ChemInform Abstract: Relaxivity Enhancement in Macromolecular and Nanosized Gd III −Based MRI Contrast Agents

ARTICLE *in* EUROPEAN JOURNAL OF INORGANIC CHEMISTRY · APRIL 2012

Impact Factor: 2.94 · DOI: 10.1002/chin.201229245

2 AUTHORS, INCLUDING:

Mauro Botta
Amedeo Avogadro University of Eastern Pi…
252 PUBLICATIONS **8,389** CITATIONS

SEE PROFILE

EurJIC European Journal of Inorganic Chemistry

MICROREVIEW

DOI: 10.1002/ejic.201101305

Relaxivity Enhancement in Macromolecular and Nanosized Gd^{III}-Based MRI Contrast Agents

Mauro Botta*[a] and Lorenzo Tei[a]

Keywords: Gadolinium / Imaging agents / Rare earths / Nanoparticles / Macromolecules

In recent years, novel, better, and more complex systems have been developed in which Gd^{III} chelates are attached to macromolecular substrates or incorporated into nanoparticles. These magnetic resonance imaging (MRI) nanoprobes make it possible to deliver to the site of interest a large number of Gd^{3+} ions, thus increasing the sensitivity of the technique. In this paper, we review the most important systems developed, the conjugation methods, and the procedures devised to optimize the relaxivity. These involve the use of Gd^{III} complexes with higher hydration number, the control of the rate of exchange of the bound water molecule(s), and the reduction of the local rotational motions of the conjugated complexes. The increase in relaxivity of the individual Gd chelates leads to significant relaxivity enhancement of the nanosized systems.

Introduction

Magnetic resonance imaging (MRI) has rapidly emerged as a prominent diagnostic clinical modality thanks to its superb spatial resolution, outstanding ability to differentiate soft tissues, and the absence of ionizing radiation during its application. The use of paramagnetic metal chelates (Gd^{III} and Mn^{II}) as contrast enhancing agents (CAs) allows considerable reduction in the relaxation times of water protons in the tissues where they are distributed, and this leads to improve the diagnosis in terms of higher specificity and better tissue characterization.[1] More than 30% of all clinical MR scans make use of Gd^{III}-based CAs. However, the efficacy of the small Gd^{III} chelates is limited, and a relatively high local concentration of CA is required to obtain the contrast needed, particularly in emerging applications such as molecular imaging.[2] In search for signal amplification strategies, it had been recognized very early that the rotational dynamics represents the main factor controlling the efficiency of the low-molecular-weight Gd^{III} chelates. Therefore, over the last 20 years different approaches have been developed to slow down the rotation of the paramagnetic complex, starting from its interaction with the most abundant blood plasma protein, human serum albumin (HSA).[3] The reversible formation of adducts with HSA

[a] Dipartimento di Scienze e Innovazione Tecnologica, Università del Piemonte Orientale "Amedeo Avogadro",
Viale T. Michel 11, 15121 Alessandria, Italy
Fax: +39-0131-360250
E-mail: mauro.botta@mfn.unipmn.it

Mauro Botta received his Laurea cum laude in Chemistry from the University of Turin under the supervision of Prof. S. Aime. In 1998 he was appointed as Associate Professor at the Università del Piemonte Orientale "Amedeo Avogadro" and promoted to a Chair in Chemistry in 2004. His research activities have focused on NMR studies of inorganic systems, starting from organometallic clusters and then moving to lanthanide complexes. Current interests are the development and NMR relaxometric characterization of paramagnetic systems as MRI probes. He has been member of COST Chemistry Actions related to MRI contrast agents since 1993, developing collaborations with Durham, Lausanne, Berkeley, and Debrecen.

Lorenzo Tei received his Laurea cum laude in Chemistry from the University of Florence, Italy, and then his Ph. D. degree in Chemistry from the University of Nottingham, UK. He was a postdoctoral fellow at the Universities of Cagliari and Torino, Italy. He was appointed Assistant Professor in Organic Chemistry at the University of Piemonte Orientale "Amedeo Avogadro" in 2006. His research interests span from the synthesis of efficient MRI contrast agents to the development of probes for MR molecular imaging applications.

represents one of the major routes to achieve high relaxation enhancement for Gd^{III} complexes as a result of the reduced rotational tumbling rate ($1/\tau_R$) of the macromolecular adduct.

In the last decade, the optimization of the relaxivity of low-molecular-weight chelates was pursued together with the development of strategies to deliver a large number of probes at the site of interest. Thus, macromolecular systems have been investigated early on, but only in recent years have we seen an explosive growth of studies involving different types of nanoparticles (NPs) bound to proteins, polymers, dendrimers, micelles, liposomes, viral capsids, metal oxides, zeolites, mesoporous silicas.[4,5]

A relevant issue is the control of the overall size of the NPs (Figure 1), since those with a mean diameter below 5 nm are usually eliminated by renal excretion, whereas larger particles (>100 nm) are taken up easily by macrophages.[6] Another advantage of these NPs is that they can incorporate different functionalities; for example, they can act as vectors for specific targeting, dyes or drugs for multimodal imaging or therapeutic delivery.

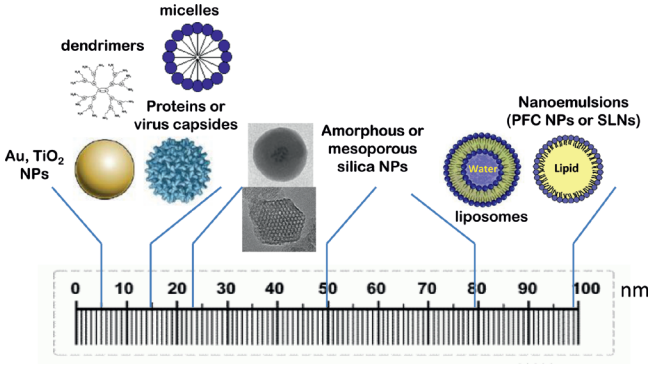

Figure 1. Macromolecular or nanosized systems used as Gd^{III} based contrast agent classified on the basis of their size.

Therefore, a careful design of structure, composition, and surface chemistry is essential to achieving the desired properties in NP-based systems, such as high imaging contrast and chemical stability, target specificity, and/or multimodality.[7] Several excellent and comprehensive reviews have discussed the preparation, properties, and applications of these nanosized CAs.[4,5]

However, the development of more efficient and sophisticated nanoprobes has only seldom been combined with an attempt at enhancing the relaxivity of the individual paramagnetic unit. This requires a proper choice of the Gd chelate and an optimization of the conjugation mode. The aim of this review is to provide a concise and critical summary of the problems associated with such relaxivity optimization and of the possible solutions explored.

Theoretical Background

The enhancement of the longitudinal and transverse nuclear magnetic relaxation rates of the water nuclei observed in the aqueous solutions of paramagnetic Gd^{III} complexes arises from the time fluctuation of the dipolar coupling between the electron magnetic moment of the metal ion and the nuclear magnetic moment of the solvent nuclei.[8] This dipolar coupling is traditionally described in terms of two mechanisms: a short-range and a long-range interaction involving the water molecules that belong to the inner coordination sphere of the metal ion (*inner-sphere* contribution, IS) and those water molecules that are not directly bound to the paramagnetic center but diffuse freely next to the complex (*outer-sphere* contribution, OS), respectively.[1] The relaxivity, r_1, defined as the relaxation enhancement normalized to a 1 mM concentration of the paramagnetic ion, can then be expressed as the sum of these two components [Equation (1)].

$$r_1 = r_1^{IS} + r_1^{OS} \tag{1}$$

The time modulation in the *inner-sphere* mechanism is provided by the molecular reorientation of the system (τ_R), the electron spin relaxation ($T_{1,2e}$), and the chemical exchange (with a mean residence lifetime $\tau_M = 1/k_{ex}$) of the bound water molecule(s). This latter process should be sufficiently fast (ca. 5–50 ns for Gd^{III} complexes) to provide an efficient means of transferring the effect to the bulk water. In the *outer-sphere* mechanism, which represents the only contribution to the relaxivity for complexes without metal-bound water molecules ($q = 0$), the electron–nuclear magnetic dipolar coupling is modulated by the relative translational diffusion of solute and solvent, D, and by the electronic relaxation times. This contribution can account for nearly 50% of the relaxivity of monoaqua ($q = 1$), low-molecular-weight Gd^{III} complexes at high fields, whereas its contribution is often negligible in the case of macromolecular systems in the approximate frequency range 10–60 MHz. The *inner-sphere* contribution, as described by the Solomon–Bloembergen–Morgan theory, can be summarized by Equations (2)–(4).

$$r_1^{IS} = \frac{p_M}{T_{1M} + \tau_M} \tag{2}$$

where P_M is the molar fraction of the bound water molecules ($P_M = [Gd^{III}]q/55.6$) and T_{1M} is the longitudinal nuclear magnetic relaxation time of the bound water protons. This latter can be simply expressed by Equations (3) and (4).

$$\frac{1}{T_{1M}} = \frac{K}{r_H^6}\left[\frac{3\tau_{C1}}{1+\omega_H^2\tau_{C1}^2} + \frac{7\tau_{C2}}{1+\omega_S^2\tau_{C2}^2}\right] \tag{3}$$

$$\frac{1}{\tau_{Ci}} = \frac{1}{\tau_R} + \frac{1}{\tau_M} + \frac{1}{T_{ie}} \qquad (i = 1,2) \tag{4}$$

where K combines a series of constants and assumes a value of 5.18×10^{-31} (cm^6/s^2; CGS unit) for Gd^{III}, r_H is the dis-

tance between the metal ion and the protons of the coordinated water molecules, ω_H and ω_S are the proton and electron Larmor frequencies, respectively. The electron spin of gadolinium(III) is characterized by fast relaxation processes (even though a few orders of magnitude slower than those for the other paramagnetic lanthanide cations), and the approximation is usually made that these can be described in terms of a single longitudinal (T_{1e}) and transverse (T_{2e}) relaxation time. Both T_{1e} and T_{2e} vary with the magnetic field strength and their field dependence is described by two parameters: Δ^2, the square of the trace of the zero-field splitting (ZFS) tensor, and τ_V, the correlation for the modulation of the transient ZFS. Under this assumption the overall correlation time is given by Equation (4).[9] The relaxivity varies with the magnetic field strength, as a consequence of the frequency dependence given by Equation (3) and that of $T_{1,2e}$. For this reason, the best way to obtain the set of parameters governing the relaxivity is through a magnetic-field-dependent study. Experimentally, this is done by measuring longitudinal relaxation rates of the water proton over a wide range of magnetic fields with a field-cycling spectrometer that rapidly switches the magnetic field strength over a range corresponding to proton Larmor frequencies of approximately 0.01–20 MHz.[10] Additional data at higher fields are measured with standard NMR spectrometers. The data points represent the so-called nuclear magnetic relaxation dispersion (NMRD) profile, which is fitted to the inner- and outer-sphere equations to yield the values of the relaxation parameters.

The issue of relaxivity enhancement is essentially related to the task of shortening T_{1M} as much as possible [Equation (2)] by optimizing the molecular parameters included in τ_{Ci} [Equation (4)] without violating the fast-exchange conditions: $T_{1M} << \tau_M$. This condition is rather straightforward in low-molecular-weight complexes, where in most cases τ_C simply needs to be lower than approximately 0.5 μs. However, in macromolecular systems T_{1M} can be more than one order of magnitude shorter, and thus the fast exchange condition requires quite short values for the mean residence lifetime, which have proven difficult to attain (vide infra). For small Gd^{III} chelates, the *inner-sphere* relaxivity at high frequencies (>10 MHz) is largely dominated by the fast rotational motion characterized by τ_R values of approximately 50–200 ps. Being 1–3 orders of magnitude shorter than the water exchange lifetime and the electron spin relaxation times, the rotational correlation time represents the effective global correlation time τ_C in Equations (3) and (4). For this reason, the NMRD profiles of low-molecular-weight complexes have in common a simple and typical behavior: a plateau in the frequency range approximately 0.01–1 MHz, a single dispersion ($\omega_S\tau_C \approx 1$) at about 6–8 MHz, and a further plateau at higher field strengths (Figure 2).[1c,11]

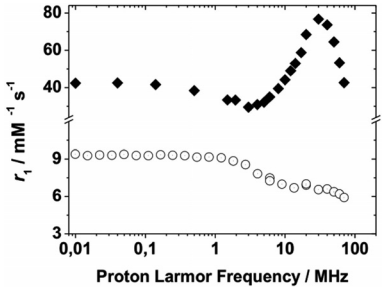

Figure 2. NMRD profiles of free (○) and HSA-bound (♦) Gd–NpEGTA (see Scheme 3) at 25 °C.

The increase in molecular dimensions while moving from small Gd^{III} chelates to nanosized systems influences directly the rotational dynamics, and then it strongly impacts the relaxivity. The τ_R values are typically in the range 0.5–50 ns and thus comparable to or even longer than τ_M and $T_{1,2e}$. As a consequence, the field dependence of the relaxivity, and therefore the shape of the NMRD profiles, changes profoundly. When the electronic relaxation time strongly influences the correlation time for the dipolar interaction [Equation (3)], its field dependence becomes visible and causes both a dispersion ($\omega_S\tau_C$) around 1–3 MHz and a typical peak in the NMRD profiles centered at approximately 20–50 MHz (Figure 2). This high-field r_{1p} peak moves to lower frequencies by slowing down the molecular tumbling (longer τ_R). Of particular relevance is also the role of the exchange lifetime τ_M of the bound water molecule. Unlike the small Gd^{III} chelates, for nanosized systems it can have a non-negligible contribution to the overall correlation time [Equation (4)] and, more importantly, it controls the efficiency of the propagation of the paramagnetic effect to the bulk of the solvent [Equation (2)].[12] Two main situations may arise: (1) $\tau_M << T_{1M}$, which defines the fast exchange condition where r_1^{IS} is not limited by the slow water exchange rate; (2) $\tau_M \geq T_{1M}$, in the intermediate/slow exchange condition the relaxivity can be severely limited by the long exchange lifetime.

For commercial Gd-based CAs and related $q = 1$ derivatives, T_{1M} assumes a value of about $3–7 \times 10^{-6}$ s (ca. 20 MHz and 298 K), and thus the fast exchange condition is achieved for $\tau_M \leq 0.2$ μs. This is the case for most of the complexes at high fields. On the other hand, in the case of macromolecular systems, T_{1M} is sensibly shorter and its value can be placed approximately in the range $9–2 \times 10^{-7}$ s, which roughly corresponds to r_1^{IS} values of 20–90 $mM^{-1} s^{-1}$. The fast exchange condition then requires τ_M to be much shorter, of the order of approximately 30 ns. Thus, it follows that, for typical macromolecular systems made up of conjugated DOTA-like or DTPA-like complexes, the intermediate/slow exchange condition is likely to occur and that the relaxivity is restricted by relatively long τ_M. For this reason, the high relaxivity values predicted by theory have been seldom achieved. The effect of different τ_M values on the NMRD profiles of slowly tumbling Gd^{III} complexes are clearly seen in Figure 3. The effects are quite large around 20–40 MHz and tend to strongly attenuate at higher fields.

Another important factor that is responsible for the limitation of r_1^{IS} below the values predicted by theory for the Gd^{III} chelates attached to large substrates is the presence of local rotational motions about the linker between the coordination cage and the anchoring site on the macro-

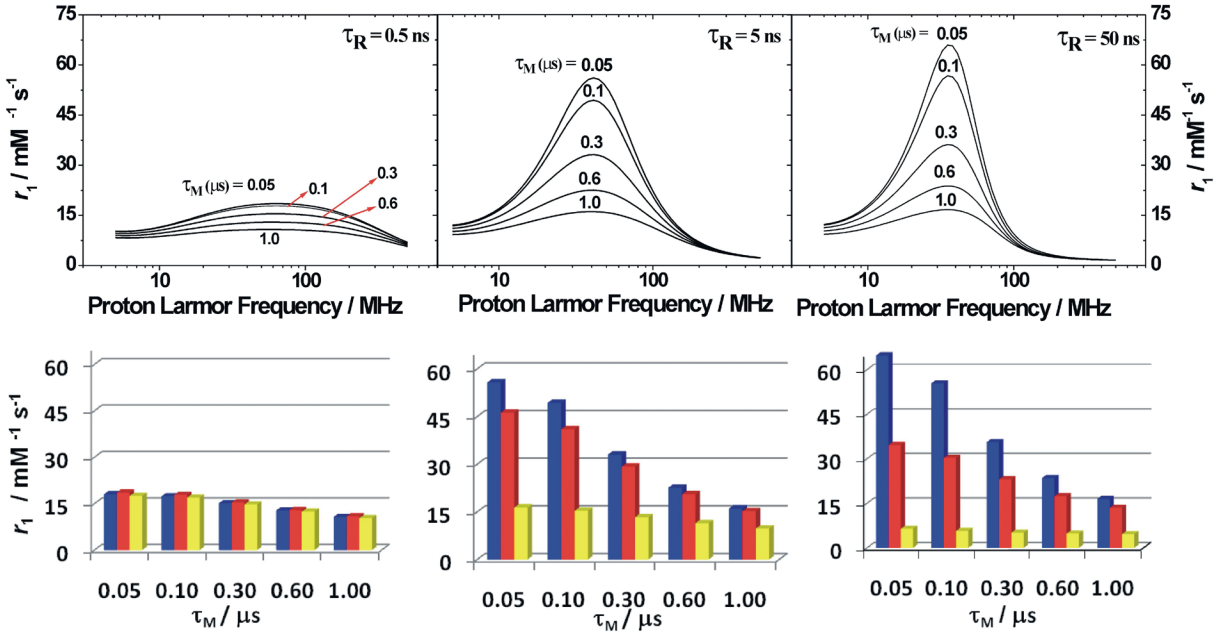

Figure 3. Top: simulated NMRD profiles showing the effect of increasing τ_M values (0.05–1.0 μs) on the high-field relaxivity of a $q = 1$ Gd^{III} system with rotational correlation times τ_R of 0.5 (left), 5.0 (middle), and 50 ns (right). Other parameters: $\Delta^2 = 3 \times 10^{19}$ s^{-2}, τ_V = 20 ps, $r = 3.0$ Å, $a = 4.0$ Å, $D = 2.24 \times 10^5$ $cm^2 s^{-1}$, $T = 298$ K. Bottom: plot of the relaxivity at 40 (blue), 60 (red), and 120 MHz (yellow) as a function of τ_M. The limiting effect of the long exchange lifetime increases by slowing down the rotation and by decreasing the magnetic field strength.

molecule. These local rotations are faster than the global tumbling motion of the whole system and result in a shorter effective τ_R and hence lower relaxivity. In such a case, the NMRD data are best analyzed by describing the rotational dynamics according to the model-free Lipari–Szabo approach.[13]

This model allows separating the contribution of the overall global rotation of the nanosized system (τ_{RG}) from the contribution of the faster local motion (τ_{RL}) due to the free rotation of the coordination cage about the pendant arm. The degree of correlation between the two types of motions is given by the parameter S^2 whose value covers the range between zero (completely independent motions) and one (totally correlated motions). In this case, Equations (3)–(4) assume the forms given in Equations (5) and (6), which are valid at high frequencies.

$$\frac{1}{T_{1M}} = \frac{K}{r_H^6}\left[\frac{3S^2\tau_{CG}}{1+\omega_H^2\tau_{CG}^2} + \frac{3(1-S^2)\tau_{CL}}{1+\omega_H^2\tau_{CL}^2}\right] \quad (5)$$

$$\frac{1}{\tau_{CG}} = \frac{1}{\tau_{RG}} + \frac{1}{\tau_M} + \frac{1}{T_{1e}}; \quad \frac{1}{\tau_{CL}} = \frac{1}{\tau_{CG}} + \frac{1}{\tau_{RL}} \quad (6)$$

In Figure 4 are reported simulated NMRD profiles relative to a macromolecular system characterized by τ_{RG} = 10 ns for different values of τ_{RL} and S^2.

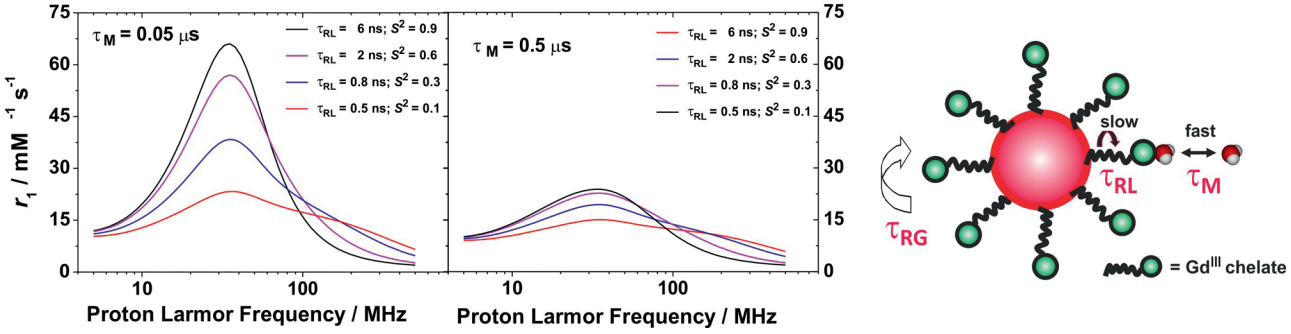

Figure 4. Left: simulated NMRD profiles showing the effect of local rotation on the relaxivity of a $q = 1$ Gd^{III} system with a global rotational correlation times τ_{RG} of 10 ns and τ_M of 50 (left) and 500 (right) ns. The local rotational correlation time τ_{RL} and the order parameter S^2 decrease from top to bottom. Other parameters: $\Delta^2 = 3 \times 10^{19}$ s^{-2}, $\tau_V = 30$ ps, $r = 3.0$ Å, $a = 4.0$ Å, $D = 2.24 \times 10^5$ $cm^2 s^{-1}$, $T = 298$ K. Right: the relaxivity of a conjugated Gd^{III} chelate depends primarily on the global molecular tumbling (τ_{RG}), the degree of internal motion (τ_{RL}), and the rate of exchange, $1/\tau_M$, of the bound water molecule(s).

Conjugation Strategies and Bifunctional Chelates

The choice of the Gd^{III} chelate to be used in the conjugation to the macromolecular or nanosized system depends both on the functional group present on the nano-object and on the properties required of the Gd^{III} chelate. Bifunctional chelating agents (BFCA) containing a polyamino polycarboxylic ligand capable of strongly coordinating the Gd^{3+} ion on one side and a functional group able to form a stable covalent bond with the carrier on the other side have been recently reviewed.[14] These agents allow the covalent linkage of the imaging reporter to the nanosystem through a large variety of chemical bonds, the most common being the amide and thiourea, obtained by reaction of an activated carboxylic acid with an amine and of a thioisocyanate with an amine, respectively. Other linkages are obtained through reaction of maleimides or disulfides with thiols, aldehydes or isocyanates with amines (reductive amination and urea formation, respectively), but also the click reaction between an alkyne and an azide, leading to 1,2,3-triazoles, has started to be widely employed as it involves very mild reaction conditions.[15] It must be also highlighted that the properties of the final conjugate can be finely tuned with the insertion of a spacer between the BFCA and the nanosized carrier. The most used spacers are PEG chains in order to increase water solubility and, on the other hand, aliphatic chains, to increase lipophilicity. The main purpose of the spacer is to modify the pharmacokinetics and biodistribution of the final probe, for example with the insertion of a biodegradable spacer. Moreover, in order to graft Gd^{III} chelates, nanoparticles often require a specific spacer, which varies with the nature of the particle. Thus, for example, in one case thiol-containing heterobifunctional linkers are used for attachment to Au nanoparticles, in another alkyltriethoxysilane groups terminating with another reactive functionality are grafted onto silica NPs.[16] The other key point to be considered is the choice of the Gd-based BFCA with optimal relaxometric properties, especially in terms of the number of coordinated water molecules and their exchange rate with the bulk. In fact, as the use of nanosized systems is a particularly important amplification method to increase the sensitivity for Gd-based CAs, the use of BFCAs that can form $q = 2$ Gd^{III} complexes gives a sensible improvement in the final relaxivity of the systems.[1] However, two possible drawbacks of $q = 2$ Gd systems are the decrease of the thermodynamic and kinetic stability due to the reduction of the number of donor atoms in the chelating ligand and the potential displacement of inner-sphere water molecules by endogenous anions or proteins. Thus, the few stable $q = 2$ Gd BFCAs that have been employed so far for the formation of macromolecular or nanosized systems are based on ligands AAZTA (6-amino-6-methylperhydro-1,4-diazepine-*N*,*N*′,*N*′′,*N*′′′-tetraacetic acid, compound **1** in Scheme 1)[17] and TREN–bis(1-Me-3,2-HOPO)–TAM [**2**, TREN = tris(2-aminoethyl)amine, HOPO = 1-Me-3,2-hydroxypyridinonate, TAM = 2,3-dihydroxyterephthalamide].[18] DO3A-based ligands **3** have also been used, but, as bidentate anions usually quench the relaxivity of Gd–DO3A-like complexes in vivo, the results obtained with these systems are often not satisfactory.[19] Another $q = 2$ Gd BFCA used in the conjugation to nanosystems is the acyclic diethylene triamine tetraacetic acid (DTTA). The main problem of Gd–DTTA derivatives **4** is related to their insufficient thermodynamic and kinetic stability for in vivo applications, although they have been demonstrated to be sufficiently stable for animal studies.[20] It should be noted that the use of $q > 1$ gadolinium chelates is restricted to those whose bound water molecules are not easily displaced by donor atoms of the protein (likely carboxylate groups) with formation of ternary complexes. The HOPO and AAZTA type of ligands meet this requirement.

DOTA and DTPA derivatives are largely employed BFCAs either for the high stability of their Gd^{III} complexes and for their availability also from commercial sources. They both form $q = 1$ Gd^{III} complexes with a wide range of k_{ex} values. In both cases, the functional group able to link the chelate to the nanocarrier can be on an α-substituted acetic arm or on the ligand backbone (**5**, **6**, and **11** in

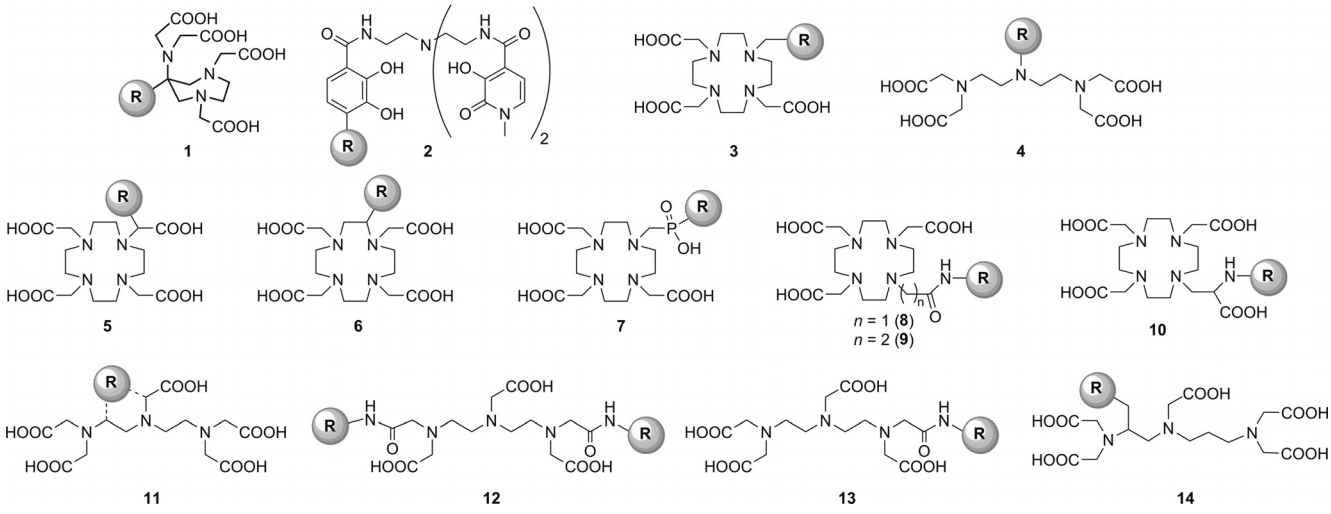

Scheme 1. Bifunctional chelates discussed in the text.

Scheme 1), thus maintaining the good relaxometric behavior of the basic Gd^{III} complexes. Different considerations are necessary for DOTA–monoamide (DOTAMA, **8**), DTPA–bisamide (compound **12**), or DTPA–monoamide (compound **13**) derivatives. The majority of publications of macromolecular or nanosized Gd-based systems contain these types of Gd^{III} chelates, mainly for their ease of preparation and for their availability from the market.[14] Unfortunately, they present some issues that make them not the ideal BFCA for these kinds of applications. First of all, Gd–DTPA–bisamide complexes are not sufficiently stable for in vivo applications, as the coordinated Gd^{3+} can be released by means of transmetallation reactions with endogenous cations.[21] In case of monoamides, it has been reported that when a carboxylic group is converted into a carboxamide for conjugation, the stability constant of the Gd^{III} complexes decreases by two to three orders of magnitude. Nevertheless, especially in Gd–DOTAMA complexes, this decrease in thermodynamic stability does not preclude the safe in vivo use of these complexes as their kinetic inertness is almost unchanged.[1c] However the low k_{ex} values in these monoamide derivatives, of the order of microseconds at 298 K (three to four times slower than those for $[Gd(DOTA)(H_2O)]^-$ or $[Gd(DTPA)(H_2O)]^{2-}$), represents a serious limiting factor for the r_1 of the corresponding macromolecular systems.

Thus, several methods to improve the water exchange rate of Gd-based BFCAs have been devised in the last decade with the aim of improving the relaxivity of the nanoconjugates. One example is the Gd^{III} complex with the monophosphinate DOTA analogue reported in Scheme 1 (compound **7**), which results in a very short τ_M (16 ns in the monomeric form) also after conjugation to a dendrimeric system thanks to the introduction of a phosphorous acid moiety in the Gd^{III} coordination sphere.[22] Moreover, the induction of a steric compression near the water coordination site was the strategy exploited in case of EPTPA derivative **14** conjugated to PAMAM dendrimers.[23] The same concept was used in case of the Gd–DOTA–propionamide complex (Scheme 1, compound **9**), which resulted in an acceleration of the k_{ex} by nearly two orders of magnitude with respect to the Gd–DOTAMA analogue.[24] Also a Gd^{III} complex with a DO3A ligand bearing a 2-aminopropionic acid pendant arm (compound **10**) takes advantage of the steric compression in order to reduce τ_M.[25] In both of these latter examples, the presence of an amino functionality suitable for conjugation allows the linkage to a variety of macromolecular platforms that are expected to show a marked enhancement of the relaxivity, no longer limited by a slow k_{ex}.

Macromolecular Systems

Proteins

Over the last twenty years, great attention has been directed to noncovalent interactions between serum proteins and bifunctional chelates containing a protein-targeting moiety and a paramagnetic unit.[3] The advantage over the covalently bound conjugates is that the reversible binding implies the constant presence of small amounts of the "free" monomeric complex that maintains its typical excretory pathway (elimination through the kidneys), thus minimizing the possible toxic effects associated with a long retention time. The noncovalent interaction favors an increased residence lifetime of the contrast agent in the vascular system, allowing for important angiographic applications of the MRI technique. In general, it is well recognized that the relaxivities of the HSA-bound complexes (r_1^b) are significantly lower than those expected on the basis of the pronounced slowing down of the molecular motion. Whereas the calculated values of r_1^b for nearly immobilized complexes are of the order of 100 $mM^{-1}s^{-1}$ (20 MHz and 298 K), the experimentally measured values fall in the range 12–55 $mM^{-1}s^{-1}$.[3] Much evidence has been collected that demonstrates that the relaxation enhancement of the inner-sphere term (r_1^{IS}) is severely limited by a relatively long exchange lifetime (τ_M) of the coordinated water molecule(s). Apart from detailed relaxometric studies, the occurrence of a slow-exchange condition is clearly illustrated by the good linear correlation between the observed r_1^b and k_{ex} values for a series of $q = 1$ DTPA- and DOTA-like Gd^{III} complexes (Figure 5a). The higher relaxivity is associated with the faster rate of water exchange, although still far from the optimal value, of a Gd–DOTA derivative bearing three pendant benzyl groups (Scheme 2).[26] A more thorough analysis of the properties of this latter complex provides important insights for further relaxivity enhancement. Let us consider five related derivatives of DOTA, containing one, two (two *cis* isomers and one *trans* isomer), and three benzyloxymethyl substituents, whose basic relaxometric properties have been previously investigated. Their r_1 values increase from Gd**L1** to Gd**L5**, simply reflecting the increase in τ_R. The water residence lifetimes, calculated from ^{17}O NMR spectroscopic data, are found to be in the range 100–250 ns, but they do not show a clear trend (Table 1).[27]

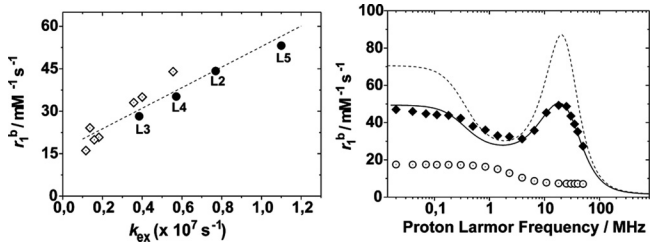

Figure 5. Left: correlation between the relaxivity values (20 MHz, 25 °C) of HSA-bound Gd^{III} complexes with $q = 1$ and their rate of water exchange. Data not labeled corresponds to data for DOTA and DTPA derivatives taken from Table 5.5 in ref.[3a] Right: NMRD profiles for Gd**L5** free (○) and bound to HSA (♦). The solid line through the experimental data was calculated with the following parameters: $\Delta^2 = 4.6 \times 10^{18}\ s^{-2}$, $\tau_V = 23$ ps, $\tau_R = 11$ ns, $\tau_M = 180$ ns, $r = 3.1$ Å, $q = 1$. The upper dashed curve is the simulated NMRD profile with $\tau_M = 41$ ns.

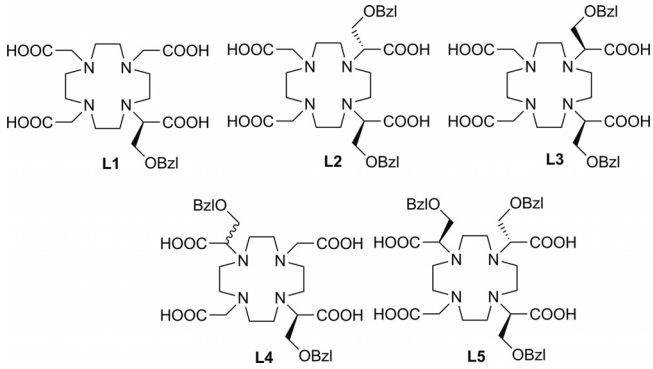

Scheme 2. DOTA–benzyloxymethyl derivatives.

Table 1. Relaxometric parameters of complexes Gd**L1**–Gd**L5**.

Complex	r_1 /mM^{-1} s^{-1}	τ_M /ns	TSAP/SAP	r_1^b /mM^{-1} s^{-1}
Gd**L1**	5.2	175	0.31	33
Gd**L2**	6.4	120	0.40	40
Gd**L3**	6.8	250	<0.1	22
Gd**L4**	6.6	200	0.19	28
Gd**L5**	7.5	102	0.59	54

On the other hand, it is well known that two diastereoisomeric pairs of enantiomers are present in the solution of Ln–DOTA complexes.[28] These are referred to as square antiprismatic (SAP or M) and twisted square antiprismatic (TSAP or m) forms. Furthermore, the water exchange rates in TSAP isomers of Gd–DOTA derivatives are about one order of magnitude faster than those of a SAP isomer. Then, the differences in the average or effective τ_M values found for Gd**L1**–Gd**L5** are likely to reflect a differential distribution of the isomers in each chelate. These distributions have been determined from the integration of the low-field axial peaks in the ^{1}H NMR spectra of the corresponding Eu^{III} complexes.[28] Knowing the isomer population makes it possible to fit the ^{17}O data to a sum of the two species, the SAP and TSAP isomers. This procedure enabled the extraction of the τ_M values for both the SAP and TSAP isomers of each complex, which are the same, within the limits of experimental error: τ_M (SAP) = 245 ± 15 ns; τ_M (TSAP) = 41 ± 2 ns. From the data in Table 1, a linear dependence of the relaxivity of the HSA-bound complexes on the isomeric ratio is evident. It is then possible to calculate the corresponding values of the hypothetical single-coordination isomers: r_1^b (SAP) ≈ 15 mM^{-1} s^{-1}; r_1^b (TSAP) ≈ 80 mM^{-1} s^{-1}. This is illustrated by Figure 5b, which shows the experimental NMRD profile of Gd**L5** bound to HSA and the simulated curve with τ_M = 41 ns. Thus, a careful selection of the coordination isomer in DOTA-like complexes may yield relaxivity values for the protein-bound adducts close to those predicted by theory.

In a recent systematic study, Caravan and co-workers have thoroughly investigated the properties of 38 Gd–DOTA derivatives and their binding to serum albumin.[29] Complexes in this series present a distinct protein-binding moiety and differ in the nature of the coordinating arm on one of the macrocyclic nitrogen atoms. At 20 MHz and 310 K, the r_1^b values were found to be in the range from approximately 12 to 56 mM^{-1} s^{-1}. The important results of this report are: (1) it is possible to modulate the water exchange rate over three orders of magnitude by the proper choice of the donor group (the relaxivities vary accordingly); (2) the second-sphere relaxivity, that is, a contribution attributable to water molecules hydrogen-bonded to the polar group of the chelator, plays a role and accounts for differences in r_1^b in similar complexes with identical donor atoms; (3) fast internal motions limit the relaxivity also in the case of complexes characterized by an optimal water exchange rate. In a related study, the importance of the second-sphere relaxivity is further highlighted and shown to be largely increased by introducing amide groups.[29b]

The presence of internal flexibility along the chain that connects the metal chelate to the targeting group represents an important limiting effect on the relaxivity of the protein-bound CA even if the other parameters have been optimized. In fact, the internal rotation about the linker does not allow the increase in molecular size to translate into a proportional decrease in the tumbling motion and hence into a relaxivity enhancement. To test the extent of such an effect on r_1^b, a simple model system consisting of a Gd^{III} complex (Gd–NpEGTA) featuring small size, compactness, a single fast exchanging bound water molecule, and a rigid targeting moiety for HSA binding (Scheme 3) was designed.[30] The rigid naphthalene backbone does not allow a high degree of local motional freedom, and only very small rotational movements of the complex in the binding pocket may take place. As a result, relaxivity values very close to those predicted by theory (68 and 78 mM^{-1} s^{-1}, at 20 and 30 MHz respectively) were achieved.

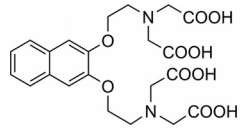

Scheme 3. NpEGTA: a naphthalene rigidified EGTA derivative.

An important approach has been discussed by Caravan et al., who combined the advantages of multimeric Gd^{III} agents with two targeting vectors.[31] The idea is that two points of attachment help to rigidify the molecule upon binding. A tetrameric Gd–DTPA-based system was functionalized with two HSA-binding moieties; it showed a large relaxivity enhancement (>30%) as compared to the related agent containing a single binding moiety. Multilocus binding greatly reduces the internal flexibility; thus, the bound complex becomes more rigid and the relaxivity increases.

Another successful strategy to enhance the relaxivity is the consideration of q = 2 complexes. Doubling the *inner-sphere* water molecules translates into a doubling of r_1^{IS}, the most relevant contribution to relaxivity in macromolecular systems. The Gd^{III}–hydroxypyridonate (Gd–HOPO) family of CAs with q = 2 exhibits optimum water exchange rates (τ_M typically 10 to 20 ns) and high thermodynamic stability (Scheme 4). A poly(ethylene glycol) (PEG) moiety of

average molecular weight 5000 Da was attached to the ligand TREN–HOPO–TAM because of the known ability of PEG chains to bind to HSA across a wide pH range.[32a] The corresponding Gd^{III} complex was found to weakly bind HSA with a formation constant $K_a = 186 \pm 50\ M^{-1}$. The relaxivity of the protein-bound complex was calculated to be $74 \pm 14\ mM^{-1}s^{-1}$ (20 MHz and 298 K), a value considerably higher than those typically reported.[32b] More recently, an analogous approach was followed by attaching a long aliphatic chain to the AAZTA coordination cage (Gd–$AAZTAC_{17}$).[33] This complex ($q = 2$ and $\tau_M = 67$ ns) was found to have a higher affinity for fatted HSA than for defatted HSA, whereas the relaxivities of the macromolecular adducts were reversed. The relaxivity of the defatted-HSA-bound complex ($r_1^b = 84\ mM^{-1}\ s^{-1}$ at 20 MHz and 298 K) is the highest value reported so far for noncovalent paramagnetic adducts with slow-tumbling substrates.

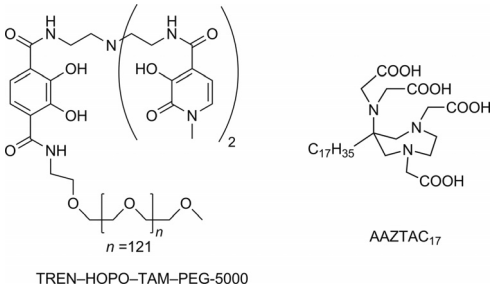

Scheme 4. HOPO and AAZTA derivatives discussed in the text.

Dendrimers

Dendrimeric systems find widespread use in a range of biomedical applications such as drug delivery, gene therapy, decontaminant agents, immunodiagnostics, and/or in vitro gene expression. These highly branched systems are characterized by a number of favorable properties: extremely low polydispersity, well-defined size and shape characteristics, nontoxicity, and ease of chemical modification.[34] For these reasons, dendrimers have also been widely explored as potential macromolecular contrast agents for MRI.[35] Among the various families of dendrimers, that of polyamidoamines (PAMAM) is one of the most studied. They consist of highly water-soluble spheroid particles with primary amino groups exposed on their surface, which are amenable to easy functionalization. The number of amino groups grows rapidly with dendrimer generation, which results in complex macromolecular architectures; there are 8 amino groups on the dendrimer of generation one (G1), 16 on G2, 32 on G3, 64 on G4, and so on.

The majority of the relaxivity values of the dendrimer conjugates are in the interval from approximately $15\ mM^{-1}s^{-1}$ to $40\ mM^{-1}s^{-1}$ (20 MHz, 298 K) depending on the type of Gd^{III} complex and dendrimer generation. These values are clearly higher than those typical of linear polymers as a consequence of the increased rigidity and nearly spherical shape of the PAMAM conjugates. As for the previously discussed macromolecular systems, the first attempt to improve the relaxivity involved the use of Gd^{III} chelates endowed with rapid water exchange from the inner coordination sphere. Pioneering work in this regard was performed by Merbach and his group. The EPTPA chelate was coupled to three different PAMAM generations (5, 7, and 9) of dendrimers through benzylthiourea linkages.[23] At 310 K and 30 MHz, the relaxivity increases from G5 to G7, and then slightly decreases for G9 (r_1 = 20.5, 28.3, and $27.9\ mM^{-1}s^{-1}$, respectively). The proton relaxivity of G5–$(Gd–EPTPA)_{111}$ is essentially limited by the marked flexibility of the dendrimeric structure. An interesting observation was made: the relaxivity has a pH dependence that originates from the pH-dependent rotational dynamics of the dendrimer skeleton. This is explained by a considerably higher τ_{RG} under acidic conditions with respect to that under basic conditions (τ_{RG} = 4.04 and 2.95 ns, respectively), which could be attributed to protonation of the tertiary amine groups in the PAMAM backbone. A phosphinate containing DTPA derivative ($DTTAP^{BnNCS}$, Scheme 5) was also conjugated to a G5 PAMAM dendrimer.[36] In the resulting system, 63 Gd^{III} chelates are conjugated to the dendrimer and the relaxivity assumes a value of $26.8\ mM^{-1}s^{-1}$ at 310 K and 20 MHz. This higher value as compared to the previous case can be attributed to the contribution of the second-sphere water molecules to the overall relaxivity.

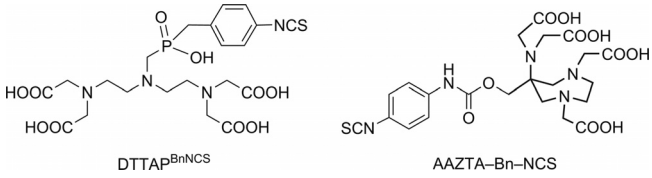

Scheme 5. Isothiocyanate functionalized BFCAs based on DTPA–phosphinate and AAZTA for the synthesis of dendrimeric CAs.

Recently, a new route was proposed for the relaxivity enhancement arising from the formation of ion pairs with large-sized substrates. A monophosphinated analogue of DOTA (DO3A–P^{ABn}, **7** in Scheme 1, R = Bn–NCS) was prepared, and its Gd^{III} chelates were covalently attached to G1–, G2–, and G4–PAMAM dendrimers through a thiourea linker. The paramagnetic conjugates showed relaxivities of 10.1, 14.1, and $18.6\ mM^{-1}s^{-1}$, respectively, at 20 MHz and 310 K.[22] The second-sphere contribution to relaxivity represents on average about 10% of the overall observed value. ^{17}O and ^1H NMR relaxometric studies confirmed that r_1 is not controlled by water exchange (τ_M ca. 45–70 ns) but by the relatively fast rotational dynamics. Whereas the molecular tumbling is sufficiently slow to attain high relaxivities (τ_{RG} increases from 1.5 to 3.1 ns), the rigidity factor S^2 (<0.3) describing the internal flexibility is far from optimum. In fact, the relaxivities per unit of mass (density of relaxivity) calculated for different G2–G5 conjugates are rather similar, which indicates that there is no clear additional benefit in loading more Gd^{III} complexes on a larger PAMAM backbone. On the other hand, r_1 shows a marked increase (e.g. by a factor of 1.8 and 1.6 for the G1 and G2 conjugates) when a positively charged polyamino acid like poly(Arg) or poly(Lys) is added to the conjugate solutions (Figure 6).[37] Since each Gd^{III} chelate bears one negative

charge, the conjugates are all polyanions, and in addition the phosphinate groups are able to set up strong hydrogen bond interactions with protonated amino groups.

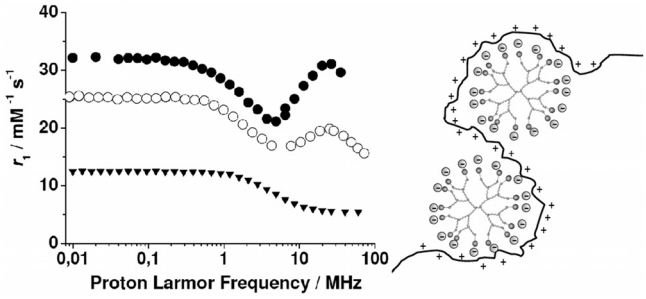

Figure 6. Left: NMRD profiles of Gd–DO3A–P^{ABn} (▼), of the G2–Gd_{16} dendrimer (○), and of the polyarginine aggregated system (●). Right: schematic representation of the electrostatic interactions between the polyamino acid and the negatively charged dendrimer.

A strand of a polyamino acid wraps around the negatively charged surface of the conjugate, thus reducing the local rotational motions of the complexes. As the effective molecular weight of the whole system increases, the global motion is also slowed down, which results in an additional increase in the relaxivity.

Only few attempts have been made to enhance the relaxivity of dendrimeric MRI contrast agents by conjugating Gd^{III} complexes with higher hydration number. The first example of a dendrimer conjugated to $q = 2$ Gd chelates concerns the case of eight Gd–AAZTA complexes functionalized with a isothiocyanate group (AAZTA–Bn–NCS, Scheme 5) bound to a PAMAM G1 dendrimer.[38] The relaxivity of this paramagnetic dendrimer is 25.0 $mM^{-1} s^{-1}$ at 298 K and 60 MHz (per Gd), a value associated with a high value of the density of relaxivity [28.2 $(g L^{-1})^{-1} s^{-1}$]. Degradable dendrimers based on esteramide (EA) and branched poly-L-lysine (PLL) were employed for the successful conjugation of up to eight $q = 2$ Gd–TREN–bis(HOPO)–TAM–ethylamine complexes. These systems exhibit high r_1 values of up to 38 $mM^{-1} s^{-1}$ at 310 K and 60 MHz.[39] Although a detailed relaxometric study is not available, the high r_1 values suggest a large degree of local rotational rigidity.

Virus Capsids

The properties of noninfectious virus capsids such as the highly ordered, nanoscale assemblies of protein molecules with a large number of chemically reactive groups on their surface have made them superb candidates as starting units for chemical modification. Viral nanosystems derived from the coat of the MS2 bacteriophage were used as platform for paramagnetic reporters. These capsids are incapable of replication, because their interior cavity is filled with host RNA rather than the viral genome. Modification of the surface of the virion linking covalently PEG chains was also exploited in order to reduce its immunogenicity.[40] The isothiocyanate derivative of DTPA was conjugated to the reactive amine side-chain groups of the capsid; then, ICP–OES measurements revealed that 514 Gd^{III} chelates per particle were attached. The high density of paramagnetic centers and slow tumbling rate of the modified MS2 capsids provided enhanced relaxivities up to 7200 $mM^{-1} s^{-1}$ per particle and a r_1 per Gd of 14.0 $mM^{-1} s^{-1}$ (1.5 T).[41] Also a bimodal agent, MS2(Gd–DTPA–ITC)$_m$(FITC)$_n$ with 360 Gd^{III} complexes per particle was prepared by using fluoresceine isothiocyanate as fluorescent dye. DOTAMA derivatives were also anchored to viral capsids by two different approaches: First, the commercially available NHS-activated DOTA was conjugated to the wild-type cowpea mosaic virus (CPMV) lysine residues to obtain a system with about 60 Gd units and a relaxivity of 46 $mM^{-1} s^{-1}$ at 1.5 T.[42] Second, the Cu^{I}-catalyzed azide–alkyne cycloaddition reaction was employed to covalently label CPMV particles with Gd–DOTAMA chelates; lysine residues on CPMV were first derivatized with azides, which were then reacted with alkyne-functionalized Gd–DOTAMA complexes to obtain 80 ± 20 Gd units per virion.[43] However, the slow water exchange rate of Gd–DOTAMA complexes prevented any increase in relaxivity expected by their immobilization on the large viral cage: the r_1 value was only 12.8 $mM^{-1} s^{-1}$ at 1.5 T.

About 90 Gd^{III} complexes of [TREN(HOPO)$_2$(TAM)]-based chelates were covalently attached either on the exterior or on the interior surfaces of MS2 capsids (Figure 7).[44] The surfaces were modified separately: the interior surface through tyrosine residues and the exterior surface through lysine moieties. High relaxivity values were measured (per Gd, 60 MHz, 25 °C): r_1 = 31.0 and 23.2 $mM^{-1} s^{-1}$ for the interior and exterior surfaces, respectively. Analysis of the NMRD profiles pointed out the relevant role of the local motion of the chelate on the relaxivity enhancement observed. The rigidity of the linker attaching the Gd^{III} complex to the substrate is the most relevant parameter that determines the relaxivity of the conjugated complexes. In addition to better r_1 enhancement and increased solubility, another significant advantage of using the internal surface of the capsids for the conjugation is the availability of the exterior surface for the installation of tissue targeting groups. Recently, a new set of Gd–HOPO-based MRI agents was prepared and attached to interior-modified cysteine residues through a rigidified linker.[45] This strategy restricts the local rotational mobility of the metal chelates and results in a greater relaxivity value: 41.2 $mM^{-1} s^{-1}$ at 60 MHz and 25 °C. Since 180 complexes were attached inside the nanosphere, the relaxivity per particle is 7416 $mM^{-1} s^{-1}$, up to 2.5-fold higher than that in the previous case.

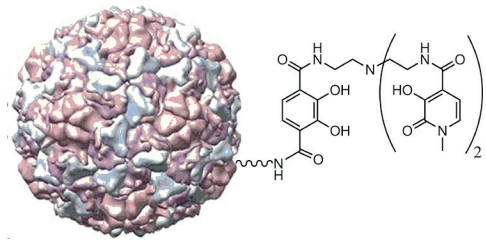

Figure 7. [TREN(HOPO)$_2$(TAM)]-based chelate covalently attached on the exterior surface of MS2 capsids.

Nanosized Systems

Micelles and Liposomes

A largely employed strategy for developing high-relaxivity systems is the use of complexes that self-aggregate into micelles or liposomes, that is, supramolecular aggregates obtained by spontaneous assembling in aqueous solution of amphiphilic molecules consisting of a hydrophobic and a hydrophilic moiety. In more detail, micellar aggregates are characterized by a unique core–shell architecture with typical size (diameter) varying between 5 and 50 nm, and they are formed when the concentration of the amphiphile, generally featuring a single aliphatic chain and a relatively large head group, is above the critical micellar concentration (cmc). On the other hand, liposomes are nanosized vesicles with diameter in the range 50 to 1000 nm. They consist of a phospholipid bilayer entrapping an aqueous core. Unilamellar vesicles, the most used liposomes, have been investigated for many years in the biomedical field, mostly as drug carriers and as models of biological membranes.

The widespread use of micelles and liposomes stems from their controlled structural properties that allow simple modulation of their pharmacokinetic properties by changing physicochemical properties such as size, surface charge, or membrane composition.[7b,46,47] In particular, liposomes are highly biocompatible, easy to prepare, and very versatile, which allows the loading of hydrophilic, amphiphilic, and lipophilic compounds. Gd-based micellar aggregates are formed by the self-assembly of an amphiphilic Gd chelate where the coordination cage is entirely exposed on the external surface of the system and thus to bulk water. On the other hand, in liposomes the Gd complexes are distributed between the inner and the outer compartment, which gives rise to two different contributions from the two types of complexes depending on the water permeability through the lipid bilayer. For example, if the membrane is permeable to water, allowing a fast water exchange rate, complexes in the inner and in the outer layer will both contribute to the observed paramagnetic relaxation rate. On the contrary, with low membrane permeability, the Gd^{III} complexes exposed to the inner compartment show a lower contribution to the overall relaxivity.[46,47] Nevertheless, the great potential of liposomes loaded with paramagnetic Gd^{III} complexes have been demonstrated in many in vivo MRI studies on animal models aimed at visualizing tumors, atherosclerotic plaques, inflammation sites, and infarcted areas of the myocardium.[48] These Gd-based lipid nanoparticles possess high molecular relaxivity resulting from both the additive effect of all of the Gd^{III} centers and the slow global rotational motion that enhances the r_1 of each paramagnetic complex. However, in spite of the high relaxivities per nanoparticle observed for these systems, the r_1 values for the individual gadolinium centers are typically modest: 10–20 $mM^{-1}s^{-1}$ at 298 K and 20 MHz, well below theoretical expectations. The two major limiting factors are again the use of neutral Gd complexes (DTPA bisamides and DOTA monoamides) exhibiting slow water exchange and/or high internal flexibility of the aggregated Gd^{III} complexes (short τ_{RL} and low S^2), which reduces the advantage associated with the high global rotation correlation time (τ_{RG}).[46]

Paramagnetic micelles with optimized water exchange have been investigated only relatively recently. The amphiphilic $[Gd(eptpa–C_{16})(H_2O)]^{2-}$ chelate was designed in order to ensure an increased k_{ex} value of the Gd^{III} complex (Scheme 6).[49] The micellar system formed by this complex shows a proton relaxivity of 22.6 $mM^{-1}s^{-1}$ (20 MHz, 298 K). This represents only a relatively modest increase in r_1, as the rotational dynamics is largely dominated by fast local motions of the lipophilic chain within the micelle. Similarly, a stable, neutral macrocyclic Gd complex based on a DOTA–monopropionamide derivative has been designed by introducing an additional methylene group in the acetic amide functionality.[24] The lipid derivative bearing a stearoyl chain (L_A, Scheme 5) aggregates and forms micelles at very low concentration (below 0.1 mM). The relaxivity of these nanoparticles (24.2 $mM^{-1}s^{-1}$; 20 MHz, 298 K) is markedly higher than that of the micelles formed by the corresponding lipophilic DOTA–monoacetamide complex L_B (15.0 $mM^{-1}s^{-1}$). The relaxivity enhancements at 20 MHz range from +130% at 278 K to +22% at 310 K. A detailed relaxometric study has shown that the large difference in the relaxivity of the aggregated complexes is entirely attributable to the large difference of the water exchange rate, whereas their rotational dynamics is strictly similar.

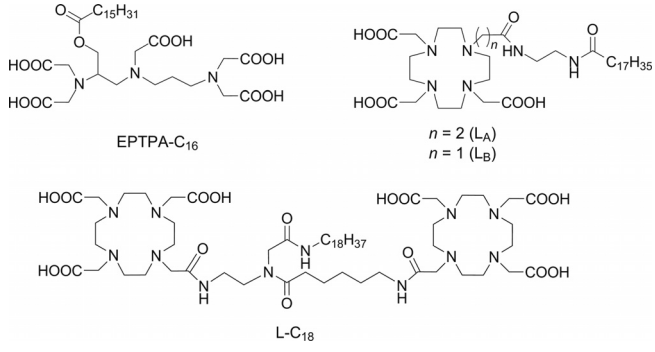

Scheme 6. Structures of EPTPA–C_{16}, L_A, L_B, and L–C_{18}.

In contrast to the previous cases, an amphiphilic conjugate of a calix[4]arene with four Gd–DOTAMA chelates aggregates in water with a cmc of 0.21 mM to give micelles with a slow water exchange rate: τ_M = 0.7 μs, at 310 K, as determined by ^{17}O NMR spectroscopy.[50] However, the system is very rigid with negligible local contributions to the overall rotational dynamics, and it has a global τ_R of 1.2 ns ($S^2 \approx 1$). The relaxivity assumes the value of 18.1 $mM^{-1}s^{-1}$ (per Gd) at 20 MHz and 310 K, limited only by the long water residence lifetime. Analogously, a dimeric complex based on two DOTAMA chelators and functionalized with an octadecyl pendant chain (Scheme 5) forms micellar assemblies with a relaxivity of 20.0 $mM^{-1}s^{-1}$ (per Gd) at 20 MHz and 310 K.[51] In comparison with the aggregated monomeric complex (GdL_B), larger values for the param-

eters τ_{RG} (30%) and τ_{RL} (48%) are calculated for Gd_2L–C_{18}, which indicates the presence of a more restricted local rotational motion. This is supported by the larger value of S^2 and could be interpreted as the consequence of larger steric interactions involving the bulkier dimeric units.

With the aim of addressing the problem of optimizing simultaneously the motional coupling between the paramagnetic unit and the nanoparticle and the rate of water exchange, we have recently reported the synthesis of a DOTA-like Gd^{III} complex functionalized with two hydrophobic chains on adjacent pendant arms.[52] In this complex, the *inner-sphere* water exchange rate is closer to the optimum range and does not limit the relaxation enhancement. The two aliphatic chains have two points of incorporation into the micelle or liposome and serve to rigidify the chelate in the bilayer [Gd–DOTA$(GAC_{12})_2$, Figure 8]. The r_1 values of the complexes embedded in liposomes and aggregated in micelles are reported in Table 2. The remarkable relaxivity gain observed (135% at 20 MHz; 99% at 60 MHz) for Gd–DOTA$(GAC_{12})_2$ relative to the monosubstituted derivative results from the marked reduction in the flexibility of the system associated with the hindered local rotation about the two aliphatic chains and thus to a reduced local rotational motion of the Gd^{III} chelate (τ_{RL}) in comparison with the global rotation of the nanoparticles (τ_{RG}). Also in case of the self-aggregation into micellar systems, the two complexes give rise to considerably different results (Table 2).

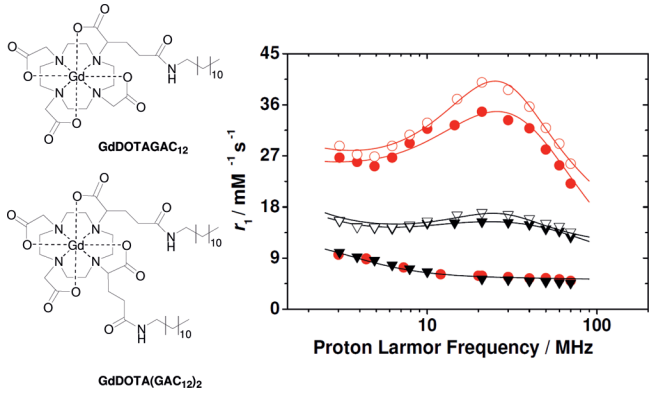

Figure 8. Left: structures of Gd–DOTAGAC$_{12}$ and DOTA-$(GAC_{12})_2$; right: NMRD profiles of Gd–DOTAGAC$_{12}$ (upside-down triangles) and Gd–DOTAGAC$_{12}$ (circles) incorporated into micelles (filled) and liposomes (open) at 25 °C. The lowest curves represent the free (non aggregated) complexes.

Table 2. Relaxometric parameters (25 °C, 20 MHz) for Gd–DOTAGAC$_{12}$ and DOTA$(GAC_{12})_2$.

	DOTAGAC$_{12}$	DOTA$(GAC_{12})_2$
r_1 /mM^{-1} s^{-1} (liposomes)	17.0	40.0
r_1 /mM^{-1} s^{-1} (micelles)	15.4	34.8
τ_{RL} /ps	210 ± 20	820 ± 110
τ_{RG} /ps	2900 ± 420	4700 ± 400
S^2	0.14 ± 0.01	0.70 ± 0.03
τ_M /ns	220 ± 8	297 ± 12

The large difference in the relaxivities of the two amphiphilic complexes (101% at 20 MHz and 298 K) is largely accounted for by their different order parameters (S^2) and τ_{RL} values.

Another important parameter that influences the *inner-sphere* relaxivity is the hydration number q. Most of the Gd-based complexes that are able to self-aggregate into micelles and liposomes are characterized by $q = 1$. Clearly, doubling the number of coordinated water molecules nearly doubles the observed relaxivity. Gd–AAZTAC$_{17}$ forms micelles (average diameter 5.5 nm) at concentrations greater than 0.1 mM, which are characterized by a relaxivity of approximately 30 mM^{-1} s^{-1} at 20 MHz and 298 K. The r_1 enhancement is significant, but the relaxivity is clearly limited by the high flexibility of the lipophilic chain ($\tau_{RG}/\tau_{RL} \geq 8.5$ and $S^2 = 0.16$). Interestingly, the relaxivity increases to 41 mM^{-1} s^{-1} when 98% of the Gd^{III} ions are replaced by diamagnetic Y^{III}.[33]

Silica Nanoparticles

The properties associated with mesoporous silica nanoparticles (MSNs), such as uniform mesopores, great functionalization capability, and significant biocompatibility, have attracted great recent attention to their biomedical applications.[5a,5d] In fact, the pore compartments and large surface area provide an ideal platform for the development of MR-enhancing materials thanks to their capability to carry a large payload of Gd units. The unique topology provides MSNs with three distinct domains that can be independently functionalized: the silica framework, the internal pores, and the external surface of the nanoparticle. Initial examples reported the attachment of Gd–DTTA complexes onto spherical MCM-41 nanoparticles (average size 75 nm)[53] or Gd–DTPA-like chelates anchored to both rodlike (100–500 nm) and spherical particles of larger dimensions (120 nm).[54] These systems were also proposed as highly efficient T_1 and T_2 CAs for cell labeling or intravascular MR imaging and, after incorporation of a fluorescent dye onto the silica, also as multimodal probes for optical imaging.

A step-by-step investigation of different mesoporous supports and MSNs surface properties, in terms of reactivity and degree of functionalization, was carried out in our laboratories in order to understand the relaxometric behavior of these hybrid materials and the nature of their potential interactions with biological tissues. First of all, the mesoporous support itself plays a significant role in the physicochemical properties of the material, as the distribution of the Gd^{III} complexes on the inner and/or outer surface is strictly dependent on the pore size and markedly influences the relaxometric properties. This was demonstrated with the synthesis of two hybrid materials based on SBA-15 and MCM-41 MSNs grafted with Gd–DOTAMA complexes.[55] The Gd–DOTAMA@MCM-41 silica showed a distribution of Gd^{III} chelates mainly on the external surface of the particles because of the limited pore diameter (ca. 25 Å), and resulted in higher r_1 as compared to that of Gd–DOTAMA@SBA-15 (pore size ca. 85 Å) as a result of

the easy accessibility of the water molecules by the paramagnetic center. Nevertheless, also for the MCM-41-based hybrid material, a fraction of the paramagnetic Gd^{III} complexes appeared silent from the relaxometric point of view, because they were partially localized inside the channels or at the entrance of the pores and were hence less exposed to the solvent. Then, the second step was the attachment of different Gd^{III} complexes onto amino-functionalized MCM-41 MSNs, that is, DOTA-like and DO3A-like chelates.[56] While the Gd–DO3A-based hybrid system resulted in poor efficiency due to the interaction of the Gd^{III} complex with the silanol surface and consequent displacement of inner-sphere water molecules, Gd^{III}–DOTAGA [DOTAGA = 2-(*R*)-2-(4,7,10-triscarboxymethyl-1,4,7,10-tetraazacyclododec-1-yl)pentanedioic acid] was anchored onto MCM-41 with a high loading but had a relaxivity per Gd lower than that expected (Figure 9). In this case, the low r_1 was attributed not only to the attachment of the chelate inside the silica channels but also to a reduced water exchange rate due to interaction of the negatively charged Gd^{III}–DOTAGA complex with protonated amino groups on the surface. For instance, the transformation of these protonated amino groups into amides resulted in a large increase of r_1 of the final material due to a threefold faster k_{ex} (from 20.3 $mM^{-1}s^{-1}$ to 37.8 $mM^{-1}s^{-1}$, per Gd), demonstrating that the surface chemistry of the mesoporous silica

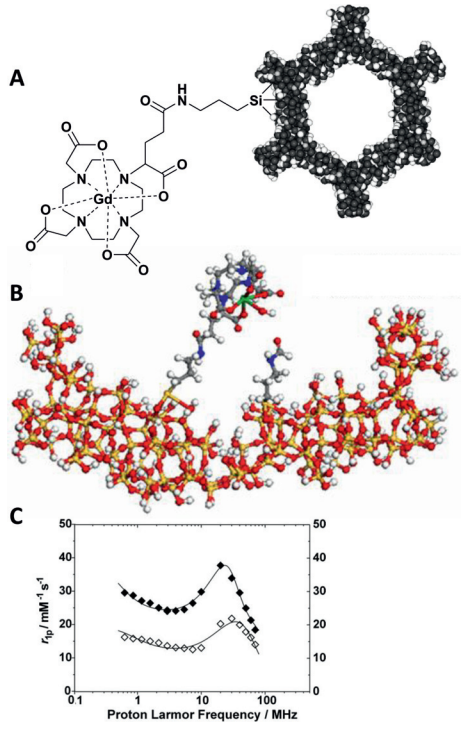

Figure 9. Schematic representation of Gd–DOTAGA grafted on mesoporous silica nanoparticles (A) and of the Gd^{III} complex/silica surface interaction after acetylation of the amino groups (B). $1/T_1$ NMRD profiles at 310 K for Gd–DOTAGA/MCM-41 before (◇) and after (♦) acetylation of the amino groups (C). Adapted with permission from ref.[56] Copyright 2010 Wiley-VCH Verlag GmbH & Co. KGaA.

can strongly influence the relaxometric properties of the nanoparticles.[56]

Finally, the synthesis of MSNs by anchoring Gd^{III} complexes only on the external surface of the mesoporous silica, which left the pores empty but available for further functionalization, resulted in even larger r_{1p} values. As observed before, transformation of the amino groups left on the particle surface into amides enhances further the relaxivity, increasing it to a value of about 80 $mM^{-1}s^{-1}$ per Gd (ca. 67200 $mM^{-1}s^{-1}$ per particle).[57]

Other Inorganic Nanoparticles Labeled with Gd^{III} Complexes

Other types of inorganic nanoparticles such as gold, titanium oxide, and nanodiamonds have been considered as carriers of Gd^{III} complexes.

Particles based on nanodiamond powder have a diameter in the range 5–20 nm and good dispersibility in aqueous solutions. Because of the extreme synthetic conditions (diamond detonation followed by treatment with oxidizing acids), the surface of a nanodiamond particle is coated with a variety of functional groups allowing for chemical modification. To synthesize a MRI nanoprobe, amine-functionalized Gd–DO3A complexes were coupled to the carboxylic acid groups on the nanodiamond surface (48 ± 3 mm of Gd^{III} per 1 $mg\,mL^{-1}$ of nanodiamond). The Gd-modified nanodiamond particles exhibited an interesting relaxivity (per Gd) of 58.8 $mM^{-1}s^{-1}$ at 1.5 T. The interaction of the water nanophase with the paramagnetic metal ion, induced by the strong electrostatic potentials on the nanodiamond facets, combined with the size of the nanodiamond aggregates (55–130 nm), were proposed to contribute to the high relaxivity of the system.[58]

An interesting approach employed DNA-labeled TiO_2 nanoconjugates functionalized with Gd^{III} complexes to allow the visualization of certain genomic sequences in cells and tissues by MRI.[59] The TiO_2 nanoparticles (3–5 nm) were surface-modified by exploiting their selective reactivity to 1,2-enediol ligands. Gd–DOTAMA complexes bearing a dopamine moiety were treated with TiO_2 nanoparticles in the presence and absence of surface-conjugated oligonucleotides. These nanoconjugates showed low relaxivity values (3.5 $mM^{-1}s^{-1}$ per Gd at 1.5 T) mainly due to the slow water exchange rate of the complex. T_1-weighted MR images were acquired on PC3M cells incubated with the nanosystem, which displayed a greater contrast over control cells.

Nanocrystals made of noble metals such as gold or silver have also been attractive candidates, as it is easier to control their size, shape, and surface chemical composition. Gold NPs are easily obtained by reducing a gold salt in the presence of Gd^{III} chelates bearing thiol functional groups. Moreover, the high electron density of these heavy-metal NPs open the possibility to use these agents for both MR and X-ray imaging.[60] For example, a dithiolated DTPA–bisamide ligand was conjugated to gold nanoparticles, anchoring about 150 ligands on 2–2.5 nm sized particles.[61] It has been demonstrated that some ligands of the organic

shell were linked to the surface by only one thiol group, which gives rise to the formation of a multilayered shell with inter- and intralayer disulfide bonds between neighboring ligands. The presence of this shell ensures good colloidal stability and enables the immobilization of a large number of Gd^{III} chelates on each particle. Nevertheless, the presence of the neutral DTPA–bisamide derivative severely limits the relaxivity of these particles, which results in a r_1 per Gd of only 3.9 $mM^{-1}s^{-1}$. A great improvement was obtained by Helm and co-workers who reported gold NPs functionalized with a thiolated DTTA derivative (q = 2) having a size distribution from 1 to 13 nm (Figure 10).[62] The NMRD profile at 298 K showed a high r_1 peak of approximately 60 $mM^{-1}s^{-1}$ at 30 MHz, corresponding to an enhancement per NP of more than 3000 $mM^{-1}s^{-1}$. The fit of the curve indicated slow rotational motion with the absence of internal rotation explained by the dense packing and the rigidity of the Gd–DTTA units on the surface of the NPs. Recently, the factors limiting the relaxivity of gold NPs functionalized with a thiolated DTPA derivative (size 2 nm) were explored by using EPR, an established method to measure the rotational dynamics of paramagnetic species.[63] Because of the insensitivity of the very broad Gd^{3+} EPR spectrum to molecular rotation, the replacement of Gd^{3+} ions with vanadyl cations (VO^{2+}), which exhibit strongly anisotropic hyperfine (A) and Zeeman (g) tensors, allowed the measurement of the molecular tumbling of the system on the sub-nanosecond time scale by EPR. This analysis suggested that the anchored Gd^{III} chelates exhibit relatively high rotational motion, which restricts their relaxivity. To improve the relaxivity of these contrast agents based on gold NPs, first the increase in the particle diameter was shown to result in lower surface curvature and hence tighter ligand packing, which in turn led to increased relaxivity. In a second approach, the gold NPs were coated with multilayers of oppositely charged polyelectrolytes. The restricted motion of Gd^{III} chelates coated by 2–4 polymer layers led to higher values of relaxivity which, though, was dramatically reduced for thicker layers, presumably due to restricted diffusion of water molecules.[63]

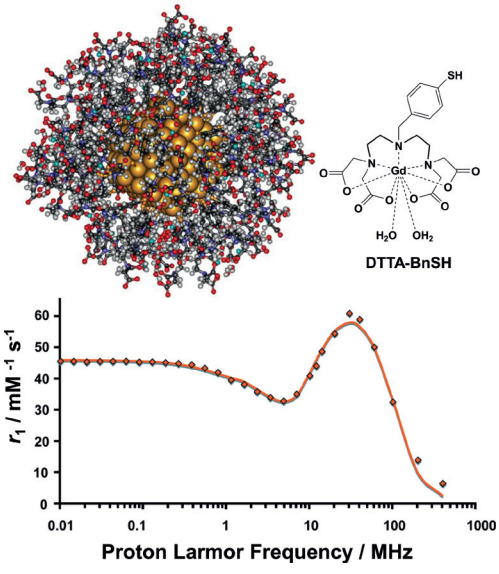

Figure 10. Top: partially optimized structure (MM3 force field) of YDTTA–BnSH@Au with the corresponding chemical structure of the Gd^{III} complex.[62] Bottom: ^1H NMRD profile for Gd–DTTA–BnSH@Au at 298 K fitted by using the modified Florence approach. Adapted with permission from ref.[62] Copyright 2009 American Chemical Society.

Conclusions

The chemistry of MRI probes has developed enormously over the last 10–15 years, and a great deal of new information is now available that enables the rational design of sophisticated systems with optimized performance. The detailed knowledge acquired on the mechanisms and factors controlling the rate of water exchange, the growing availability of stable Gd^{III} chelates with an expanded first hydration shell, and new emerging strategies to attenuate the problem of the extensive rotational flexibility of the linker between the complex and the macromolecular substrate, all contribute to enhance the relaxivity (Table 3). Moreover, given the large number of monomeric Gd^{III} complexes covalently or noncovalently bound to a macromolecule or incorporated into a nanoparticle, what might seem like a relatively modest increment of r_1 per Gd actually can translate into a huge gain per particle. Further advances in the exploration of novel systems in which the paramagnetic units are confined into small cavities, new insights into the mechanism of action of Gadofullerenes[66] and Gadonanotubes[67] could represent a relevant breakthrough and substantially expand the sensitivity limits of the MRI technique.

Table 3. Relaxivity values of selected Gd^{III} chelates conjugated to different macromolecular substrates and nanoparticles.

Gd^{III} chelate	Substrate	r_1 /$mM^{-1}s^{-1}$	ν /MHz	T /°C	Ref.
L5	Poly-β-CD	49	20	25	[64]
L5	HSA	54	20	25	[26]
NpEGTA	HSA	78	30	25	[30a]
$AAZTAC_{17}$	HSA	84	20	25	[33]
DOTA–1f	HSA	55.5	20	37	[29a]
G2–$(7)_{16}$/polyarginine	dendrimer	30.8	20	25	[37]
G7–$(EPTPA)_{111}$	dendrimer	25.1	20	25	[23]
$TREN(HOPO)_2TAM$	MS2 capsid external	23.2	60	25	[44]
$TREN(HOPO)_2TAM$	MS2 capsid internal	31.0	60	25	[44]
$TREN(HOPO)_2TAM$	MS2 capsid internal	41.2	60	25	[45]
HPDO3A	apoferritin	ca. 80	20	25	[65]
L_A	micelle	24.2	20	25	[24]
DOTA–calix[4]arene	micelle	18.1	20	37	[50]
$DOTA(GAC_{12})_2$	micelle	34.8	20	25	[52]
$AAZTAC_{17}$	micelle	30	20	25	[33]
$DOTA(GAC_{12})_2$	liposome	40.0	20	25	[52]
DOTAGA	MSNs	20.3	20	25	[56]
DOTAGA	MSNs after acetylation	37.8	20	25	[52]
DTTA–BnSH	AuNPs	ca. 60	30	25	[62]

In fact, the sensitivity of detection of MRI is, as expected, lower than that of other imaging techniques. Therefore, to compensate for this intrinsic limitation, the MRI probes need either to contain a large number of paramagnetic chelates or to target high-density receptors. Fibrin or extracellular matrix components represent an example of high-concentration targets that have been successfully detected by MRI with use of a gadolinium multimer conjugated to a fibrin-specific peptide.[68] On the other hand, the visualization of molecular epitopes present at nanomolar concentrations by MRI requires the use of nanoprobes. For example, it has been shown that a perfluorocarbon nanoparticle containing a high payload of Gd^{3+} ions (>90000/particle) can provide a degree of contrast of diagnostic relevance in the picomolar range.[69] Several other examples have been reported of the in vivo use of T_1 Gd-based nanoprobes, including Gd systems based on PAMAM dendrimers,[70] paramagnetic liposomes,[48,71] or Gd-loaded proteins such as apoferritin or LDL.[72,73]

However, it has to be outlined that most of the reported nanosized MRI probes are simply model systems in the stage of in vitro testing or, at most, used in preliminary animal studies. Before clinical translation, several properties have to be taken into consideration and optimized: stability, biodegradability, excretion pathways, toxicity. Various surface modification methods have been devised in order to ensure a good solubility in water, high colloidal stability, efficient clearance from the body, and thus lower potential toxicity. Often, hydrophilic groups are introduced onto the surface of the nanoparticles to make them more water-dispersible and biocompatible. To this end, several physicochemical properties of the paramagnetic NPs need to be properly controlled. Among these, particularly relevant are size (i.e. hydrodynamic diameter, HD), hydrophobic character, and overall surface charge. Finally, the possible toxicity of the NPs, in particular inorganic NPs, is an issue of obvious relevance that could hamper their use in preclinical in vivo studies and clinical protocols. Thus, a highly interdisciplinary approach will be needed to guide the further development of these innovative systems from the laboratory bench to real biomedical applications.[74]

Acknowledgments

The authors thank Regione Piemonte (PIIMDMT and Nano-IGT projects) and Ministero dell'Università e della Ricerca (MIUR) (PRIN 2009) for support. Most of this work was performed within the frame of European Union Actions COST-D18 and COST-D38. The collaboration with Prof. Silvio Aime and his group (University of Turin) is gratefully acknowledged.

[1] a) A. E. Merbach, È. Tóth, *The Chemistry of Contrast Agents in Medical Magnetic Resonance Imaging*, John Wiley & Sons, Chichester, **2001**; b) S. Aime, M. Botta, E. Terreno, *Adv. Inorg. Chem.* **2005**, *57*, 173–237; c) P. Caravan, J. J. Ellison, T. J. McMurry, R. B. Lauffer, *Chem. Rev.* **1999**, *99*, 2293–2352.

[2] a) E. Terreno, D. Delli Castelli, A. Viale, S. Aime, *Chem. Rev.* **2010**, *110*, 3019–3042; b) S. Aime, D. Delli Castelli, S. Geninatti Crich, E. Gianolio, E. Terreno, *Acc. Chem. Res.* **2009**, *42*, 822–831; c) S. Aime, S. Geninatti Crich, E. Gianolio, G. B. Giovenzana, L. Tei, E. Terreno, *Coord. Chem. Rev.* **2006**, *250*, 1562–1579.

[3] a) S. Aime, M. Botta, M. Fasano, E. Terreno in *The Chemistry of Contrast Agents in Medical Magnetic Resonance Imaging* (Eds.: A. E. Merbach, È. Tóth), John Wiley & Sons, Chichester, **2001**, ch. 5; b) P. Caravan, *Acc. Chem. Res.* **2009**, *42*, 851–862.

[4] a) A. J. L. Villaraza, A. Bumb, M. W. Brechbiel, *Chem. Rev.* **2010**, *110*, 2921–2959; b) D. Delli Castelli, E. Gianolio, S. Geninatti Crich, E. Terreno, S. Aime, *Coord. Chem. Rev.* **2008**, *252*, 2424–2443; c) E. J. Werner, A. Datta, C. J. Jocher, K. N. Raymond, *Angew. Chem.* **2008**, *120*, 8696; *Angew. Chem. Int. Ed.* **2008**, *47*, 8568–8580.

[5] a) T. D. Schladt, K. Schneider, H. Schild, W. Tremel, *Dalton Trans.* **2011**, *40*, 6315–6343; b) C. Khemtong, C. W. Kessinger, J. Gao, *Chem. Commun.* **2009**, 3497–3510; c) F. Hu, H. M. Joshi, V. P. Dravid, T. J. Meade, *Nanoscale* **2010**, *2*, 1884–1891; d) H. B. Na, T. Hyeon, *J. Mater. Chem.* **2009**, *19*, 6267–6273.

[6] a) D. Peer, J. M. Karp, S. Hong, O. C. Farokhzad, R. Margalit, R. Langer, *Nat. Nanotechnol.* **2007**, *2*, 751–760; b) C. Sun, J. S. H. Lee, M. Zhang, *Adv. Drug Delivery Rev.* **2008**, *60*, 1252–1265.

[7] a) J. Gao, H. Gu, B. Xu, *Acc. Chem. Res.* **2009**, *42*, 1097–1107; b) W. J. M. Mulder, G. J. Strijkers, G. A. F. Van Tilborg, D. P. Cormode, Z. A. Fayad, K. Nicolay, *Acc. Chem. Res.* **2009**, *42*, 904–914; c) C. Fang, M. Zhang, *J. Mater. Chem.* **2009**, *19*, 6258–6266; d) J. Kim, Y. Piao, T. Hyeon, *Chem. Soc. Rev.* **2009**, *38*, 372–390.

[8] L. Banci, I. Bertini, C. Luchinat, *Nuclear and Electronic Relaxation*, Wiley-VCH, Weinheim, **1991**.

[9] a) J. Kowalewski, D. Kruk, G. Parigi, *Adv. Inorg. Chem.* **2005**, *57*, 41–104; b) L. Helm, *Prog. Nucl. Magn. Res. Sp.* **2006**, *49*, 45–64.

[10] S. H. Koenig, R. D. Brown III, *Prog. Nucl. Magn. Reson. Spectrosc.* **1990**, *22*, 487–567.

[11] S. Aime, M. Botta, M. Fasano, E. Terreno, *Chem. Soc. Rev.* **1998**, *27*, 19–29.

[12] a) S. Aime, M. Botta, M. Fasano, E. Terreno, *Acc. Chem. Res.* **1999**, *32*, 941–949; b) L. Helm, G. M. Nicolle, A. E. Merbach, *Adv. Inorg. Chem.* **2005**, *57*, 327–379.

[13] a) G. Lipari, S. Szabo, *J. Am. Chem. Soc.* **1982**, *104*, 4546–4559; b) G. Lipari, S. Szabo, *J. Am. Chem. Soc.* **1982**, *104*, 4559–4570.

[14] A. Barge, G. Cravotto, G. B. Giovenzana, L. Lattuada, L. Tei, *Chem. Soc. Rev.* **2011**, *40*, 3019–3049; L. Frullano, P. Caravan, *Curr. Org. Synth.* **2011**, *8*, 535–565.

[15] J. E. Moses, A. D. Moorhouse, *Chem. Soc. Rev.* **2007**, *36*, 1249–1262.

[16] N. Erathodiyil, J. Y. Ying, *Acc. Chem. Res.* **2011**, *44*, 925–935.

[17] A. Datta, K. N. Raymond, *Acc. Chem. Res.* **2009**, *42*, 938–947.

[18] a) S. Aime, L. Calabi, C. Cavallotti, E. Gianolio, G. B. Giovenzana, P. Losi, A. Maiocchi, G. Palmisano, M. Sisti, *Inorg. Chem.* **2004**, *43*, 7588–7590; b) G. Gugliotta, M. Botta, G. B. Giovenzana, L. Tei, *Bioorg. Med. Chem. Lett.* **2009**, *19*, 3442–3444.

[19] a) M. Botta, S. Aime, A. Barge, G. Bobba, R. S. Dickins, D. Parker, E. Terreno, *Chem. Eur. J.* **2003**, *9*, 2102–2109; b) E. Terreno, M. Botta, P. Boniforte, C. Bracco, L. Milone, D. Mondino, F. Uggeri, S. Aime, *Chem. Eur. J.* **2005**, *11*, 5531–5537; c) S. Aime, E. Gianolio, E. Terreno, G. B. Giovenzana, R. Pagliarin, M. Sisti, G. Palmisano, M. Botta, M. P. Lowe, D. Parker, *J. Biol. Inorg. Chem.* **2000**, *5*, 488–497.

[20] J. M. Idee, M. Port, I. Raynal, M. Schaefer, S. Le Greneur, C. Corot, *Fund. Clin. Pharm.* **2006**, *20*, 563–576.

[21] P. L. de Sousaay, J. B. Livramento, L. Helm, A. E. Merbach, W. Meme, B.-T. Doan, J.-C. Beloeil, M. I. M. Pratae, A. C. Santos,

C. F. G. C. Geraldes, E. Toth, *Contrast Media Mol. Imaging* **2008**, *3*, 78–85.
[22] J. Rudovsky, P. Hermann, M. Botta, S. Aime, I. Lukes, *Chem. Commun.* **2005**, 2390–2392.
[23] S. Laus, A. Sour, R. Ruloff, E. Toth, A. E. Merbach, *Chem. Eur. J.* **2005**, *11*, 3064.
[24] L. Tei, G. Gugliotta, Z. Baranyai, M. Botta, *Dalton Trans.* **2009**, 9712–9714.
[25] M. F. Ferreira, A. F. Martins, J. A. Martins, P. M. Ferreira, E. Toth, C. F. G. C. Geraldes, *Chem. Commun.* **2009**, 6475–6476.
[26] S. Aime, M. Botta, M. Fasano, S. Geninatti Crich, E. Terreno, *J. Biol. Inorg. Chem.* **1996**, *1*, 312–319.
[27] M. Botta, Abstracts of the 10th International Conference on Bioinorganic Chemistry, *J. Inorg. Biochem.* **2001**, *86*, 25.
[28] a) S. Aime, M. Botta, G. Ermondi, *Inorg. Chem.* **1992**, *31*, 4291; b) S. Hoeft, K. Roth, *Chem. Ber.* **1993**, *126*, 869; c) S. Aime, M. Botta, M. Fasano, M. P. M. Marques, C. F. G. C. Geraldes, D. Pubanz, A. E. Merbach, *Inorg. Chem.* **1997**, *36*, 2059–2068.
[29] a) S. Dumas, V. Jacques, W. C. Sun, J. S. Troughton, J. T. Welch, J. M. Chasse, H. Schmitt-Willich, P. Caravan, *Invest. Radiol.* **2010**, *45*, 600–612; b) V. Jacques, S. Dumas, W. C. Sun, J. S. Troughton, M. T. Greefield, P. Caravan, *Invest. Radiol.* **2010**, *45*, 613–624.
[30] a) S. Avedano, L. Tei, A. Lombardi, G. B. Giovenzana, S. Aime, D. Longo, M. Botta, *Chem. Commun.* **2007**, 4726–4728; b) M. Botta, S. Avedano, G. B. Giovenzana, A. Lombardi, D. Longo, C. Cassino, L. Tei, S. Aime, *Eur. J. Inorg. Chem.* **2011**, 802–810.
[31] Z. Zhang, M. T. Greenfield, M. Spiller, T. J. McMurry, R. B. Lauffer, P. Caravan, *Angew. Chem.* **2005**, *117*, 6924; *Angew. Chem. Int. Ed.* **2005**, *44*, 6766.
[32] a) S. Azegami, A. Tsuboi, T. Izumi, M. Hirata, P. L. Dubin, B. Wang, E. Kokufta, *Langmuir* **1999**, *15*, 940–947; b) D. M. J. Doble, M. Botta, J. Wang, S. Aime, A. Barge, K. N. Raymond, *J. Am. Chem. Soc.* **2001**, *123*, 10758–10759.
[33] E. Gianolio, G. B. Giovenzana, D. Longo, I. Longo, I. Menegotto, S. Aime, *Chem. Eur. J.* **2007**, *13*, 5785–5797.
[34] G. R. Newkome, C. N. Moorefield, F. Vogtle, *Dendrimers and Dendrons: Concepts, Syntheses, Applications*, Wiley-VCH, Weinheim, **2001**.
[35] a) S. Langereis, A. Dirksen, T. M. Hackeng, M. H. P. van Genderen, E. W. Meijer, *New J. Chem.* **2007**, *31*, 1152–1160; b) V. J. Venditto, C. A. S. Regino, M. W. Brechbiel, *Mol. Pharmacol.* **2005**, *2*, 302.
[36] P. Lebduskova, A. Sour, L. Helm, E. Toth, J. Kotek, I. Lukes, A. E. Merbach, *Dalton Trans.* **2006**, 3399–3406.
[37] J. Rudovsky, M. Botta, P. Hermann, K. I. Hardcastle, I. Lukes, S. Aime, *Bioconjugate Chem.* **2006**, *17*, 975–987.
[38] G. Gugliotta, M. Botta, L. Tei, *Org. Biomol. Chem.* **2010**, *8*, 4569–4574.
[39] W. C. Floyd III, P. J. Klemm, D. E. Smiles, A. C. Kohlgruber, V. C. Pierre, J. L. Mynar, J. M. J. Frechet, K. N. Raymond, *J. Am. Chem. Soc.* **2011**, *133*, 2390–2393.
[40] a) Q. Wang, T. Lin, L. Tang, J. E. Johnson, M. G. Finn, *Angew. Chem.* **2002**, *114*, 477; *Angew. Chem. Int. Ed.* **2002**, *41*, 459–462; K. S. Raja, Q. Wang, M. J. Gonzalez, M. Manchester, J. E. Johnson, M. G. Finn, *Biomacromolecules* **2003**, *4*, 472–476.
[41] E. A. Anderson, S. Isaacman, D. S. Peabody, E. Y. Wang, J. W. Canary, K. Kirshenbaum, *Nano Lett.* **2006**, *6*, 1160–1164.
[42] L. Liepold, S. Anderson, D. Willits, L. Oltrogge, J. A. Frank, T. Douglas, M. Young, *Magn. Reson. Med.* **2007**, *58*, 871–879.
[43] D. E. J. Prasuhn, R. M. Yeh, A. Obenaus, M. Manchester, M. G. Finn, *Chem. Commun.* **2007**, *12*, 1269–1271.
[44] a) J. M. Hooker, A. Datta, M. Botta, K. N. Raymond, M. B. Francis, *Nano Lett.* **2007**, *7*, 2207–2210; b) A. Datta, J. M. Hooker, M. Botta, M. B. Francis, K. N. Raymond, *J. Am. Chem. Soc.* **2008**, *130*, 2546–2552.
[45] P. D. Garimella, A. Datta, D. W. Romanini, K. N. Raymond, M. B. Francis, *J. Am. Chem. Soc.* **2011**, *133*, 14704–14709.
[46] A. Accardo, D. Tesauro, A. Luigi, C. Pedone, G. Morelli, *Coord. Chem. Rev.* **2009**, *253*, 2193–2213; W. J. M. Mulder, G. J. Strijkers, G. A. F. Van Tilborg, A. W. Griffioen, K. Nicolay, *NMR Biomed.* **2006**, *19*, 142–164.
[47] E. Terreno, D. Delli Castelli, C. Cabella, W. Dastrù, A. Sanino, J. Stancanello, L. Tei, S. Aime, *Chem. Biodiversity* **2008**, *5*, 1901–1912.
[48] W. J. Mulder, G. J. Strijkers, J. W. Habets, E. J. Bleeker, D. W. van der Schaft, G. Storm, G. A. Koning, A. W. Griffioen, K. Nicolay, *FASEB J.* **2005**, *19*, 2008; W. J. M. Mulder, K. Douma, G. A. Koning, M. A. van Zandvoort, E. Lutgens, M. J. Daemen, K. Nicolay, G. J. Strijkers, *Magn. Reson. Med.* **2006**, *55*, 1170; D. A. Sipkins, K. Gijbels, F. D. Tropper, M. Bednarski, K. C. Li, L. Steinman, *J. Neuroimmunol.* **2000**, *104*, 1; W. J. Chu, T. Simor, G. A. Elgavish, *NMR Biomed.* **1997**, *10*, 87.
[49] S. Torres, J. A. Martins, J. P. Andre, C. F. G. C. Geraldes, A. E. Merbach, E. Toth, *Chem. Eur. J.* **2006**, *12*, 940–948.
[50] D. Schuehle, M. Polasek, I. Lukes, T. Chauvin, E. Toth, J. Schatz, U. Hanefeld, M. Stuart, J. Peters, *Dalton Trans.* **2010**, *39*, 185–191.
[51] L. Tei, G. Gugliotta, S. Avedano, G. B. Giovenzana, M. Botta, *Org. Biomol. Chem.* **2009**, *7*, 4406–4414.
[52] F. Kielar, L. Tei, E. Terreno, M. Botta, *J. Am. Chem. Soc.* **2010**, *132*, 7836–7837.
[53] K. M. L. Taylor, J. S. Kim, W. J. Rieter, H. An, W. Lin, W. Lin, *J. Am. Chem. Soc.* **2008**, *130*, 2154–2155.
[54] J. Kim, H. S. Kim, N. Lee, T. Kim, H. Kim, T. Yu, I. C. Song, W. K. Moon, T. Hyeon, *Angew. Chem.* **2008**, *120*, 8566; *Angew. Chem. Int. Ed.* **2008**, *47*, 8438–8441.
[55] F. Carniato, L. Tei, W. Dastrù, L. Marchese, M. Botta, *Chem. Commun.* **2009**, 1246–1248.
[56] F. Carniato, L. Tei, M. Cossi, L. Marchese, M. Botta, *Chem. Eur. J.* **2010**, *16*, 10727–10734.
[57] F. Carniato, L. Tei, A. Arrais, L. Marchese, M. Botta, *Adv. Funct. Mater.*, to be submitted.
[58] L. M. Manus, D. J. Mastarone, E. A. Waters, X.-Q. Zhang, E. A. Schultz-Sikma, K. W. MacRenaris, D. Ho, T. J. Meade, *Nano Lett.* **2010**, *10*, 484–489.
[59] P. J. Endres, T. Paunesku, S. Vogt, T. J. Meade, G. E. Woloschak, *J. Am. Chem. Soc.* **2007**, *129*, 15760–15761.
[60] C. Alric, J. Taleb, G. Le Duc, C. Mandon, C. Billotey, A. Le Meur-Herland, T. Brochard, F. Vocanson, M. Janier, P. Perriat, S. Roux, O. Tillement, *J. Am. Chem. Soc.* **2008**, *130*, 5908–5915.
[61] P.-J. Debouttiere, S. Roux, F. Vocanson, C. Billotey, O. Beuf, A. Favre-Reguillon, Y. Lin, S. Pellet-Rostaing, R. Lamartine, P. Perriat, O. Tillement, *Adv. Funct. Mater.* **2006**, *16*, 2330–2339.
[62] L. Moriggi, C. Cannizzo, E. Dumas, C. R. Mayer, A. Ulianov, L. Helm, *J. Am. Chem. Soc.* **2009**, *131*, 10828–10829.
[63] M. F. Warsi, V. Chechik, *Phys. Chem. Chem. Phys.* **2011**, *13*, 9812–9817.
[64] S. Aime, M. Botta, F. Fedeli, E. Gianolio, E. Terreno, P. L. Anelli, *Chem. Eur. J.* **2001**, *7*, 5262–5269.
[65] S. Aime, L. Frullano, S. Geninatti Crich, *Angew. Chem.* **2002**, *114*, 1059; *Angew. Chem. Int. Ed.* **2002**, *41*, 1017–1019.
[66] R. D. Bolskar, *Nanomedicine (London, U.K.)* **2008**, *3*, 201–213.
[67] K. B. Hartman, S. Laus, R. D. Bolskar, R. Muthupillai, L. Helm, E. Toth, A. E. Merbach, L. J. Wilson, *Nano Lett.* **2008**, *8*, 415–419.
[68] S. A. Nair, A. F. Kolodziej, G. Bhole, M. T. Greenfield, T. J. McMurry, P. Caravan, *Angew. Chem.* **2008**, *120*, 4996; *Angew. Chem. Int. Ed.* **2008**, *47*, 4918–4921.
[69] A. M. Morawski, P. M. Winter, K. C. Crowder, S. D. Caruthers, R. W. Fuhrhop, M. J. Scott, J. D. Robertson, D. R. Abendschein, G. M. Lanza, S. A. Wickline, *Magn. Reson. Med.* **2004**, *51*, 480–486.
[70] W. Zhu, B. Okollie, Z. M. Bhujwalla, D. Artemov, *Magn. Reson. Med.* **2008**, *59*, 679–685.

[71] C. Grange, S. Geninatti Crich, G. Esposito, D. Alberti, L. Tei, B. Bussolati, S. Aime, G. Camussi, *Cancer Res.* **2010**, *70*, 2180–2190.
[72] S. Geninatti Crich, B. Bussolati, L. Tei, C. Grange, G. Esposito, S. Lanzardo, G. Camussi, S. Aime, *Cancer Res.* **2006**, *66*, 9196–9201.
[73] S. Geninatti Crich, S. Lanzardo, D. Alberti, S. Belfiore, A. Ciampa, G. B. Giovenzana, C. Lovazzano, R. Pagliarin, S. Aime, *Neoplasia* **2007**, *9*, 1046–1056.
[74] a) T. L. Doane, C. Burda *Chem. Soc. Rev.* **2012**, DOI: 10.1039/c2cs15261d; b) T. Lammers, S. Aime, W. E. Hennink, G. Storm, F. Kiessling, *Acc. Chem. Res.* **2011**, *44*, 1029–1038; c) J. V. Jokerst, S. S. Gambhir, *Acc. Chem. Res.* **2011**, *44*, 1050–1060.
Received: November 22, 2011
Published Online: March 15, 2012

